JCTC Journal of Chemical Theory and Computation

ARTICLE

pubs.acs.org/JCTC

Micellization Studied by GPU-Accelerated Coarse-Grained Molecular Dynamics

Benjamin G. Levine,[†,▽] David N. LeBard,[†,▽] Russell DeVane,[‡] Wataru Shinoda,[§] Axel Kohlmeyer,[†] and Michael L. Klein*[,†]

[†]Institute for Computational Molecular Science and Department of Chemistry, Temple University, Philadelphia, Pennsylvania 19122, United States

[‡]The Procter & Gamble Company, Cincinnati, Ohio 45253, United States

[§]National Institute of Advanced Industrial Science and Technology (AIST), Tsukuba, Ibaraki, Japan

Supporting Information

ABSTRACT: The computational design of advanced materials based on surfactant self-assembly without ever stepping foot in the laboratory is an important goal, but there are significant barriers to this approach, because of the limited spatial and temporal scales accessible by computer simulations. In this paper, we report our work to bridge the gap between laboratory and computational time scales by implementing the coarse-grained (CG) force field previously reported by Shinoda et al. [Shinoda, W.; DeVane, R.; Klein, M. L. *Mol. Simul.* **2007**, *33*, 27−36] into the HOOMD-Blue graphical processing unit (GPU)-accelerated molecular dynamics (MD) software package previously reported by Anderson et al. [Anderson, J. A.; Lorenz, C. D.; Travesset, A. *J. Comput. Phys.* **2008**, *227*, 5342−5359]. For a system of 25 750 particles, this implementation provides performance on a single GPU, which is superior to that of a widely used parallel MD simulation code running on an optimally sized CPU-based cluster. Using our GPU setup, we have collected 0.6 ms of MD trajectory data for aqueous solutions of 7 different nonionic polyethylene glycol (PEG) surfactants, with most of the systems studied representing ∼1 000 000 atoms. From this data, we calculated various properties as a function of the length of the hydrophobic tails and PEG head groups. Specifically, we determined critical micelle concentrations (CMCs), which are in good agreement with experimental data, and characterized the size and shape of micelles. However, even with the microsecond trajectories employed in this study, we observed that the micelles composed of relatively hydrophobic surfactants are continuing to grow at the end of our simulations. This suggests that the final micelle size distributions of these systems are strongly dependent on initial conditions and that either longer simulations or advanced sampling techniques are needed to properly sample their equilibrium distributions. Nonetheless, the combination of coarse-grained modeling and GPU acceleration marks a significant step toward the computational prediction of the thermodynamic properties of slowly evolving surfactant systems.

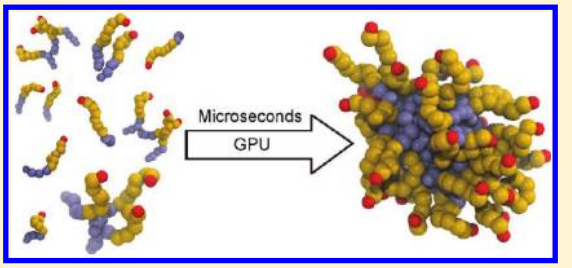

1. INTRODUCTION

Self-assembly, whereby solutions of amphiphilic molecules spontaneously order themselves into more-complex structures, is a rich and important physical phenomenon.[3,4] In addition to playing a vital role in biology and in many industrial and consumer applications, self-assembly has been harnessed to create human-designed nanostructures and functional materials.[5,6] Over the last 20 years, computer simulation has emerged as an important method to study self-assembly processes.[7−14] Recent simulation studies have addressed the properties of micellar[15−26] and reverse micellar[27−29] solutions, as well as more-complex phases[9,30−36] and dynamical behaviors.[37,38] Molecular dynamics (MD) techniques have been applied to examine self-assembled macromolecular materials as well, such as those composed of multiblock copolymers[39] and tethered nanoparticles.[40]

While much progress has been made, the quantitative prediction of the thermodynamic and kinetic properties of self-assembled solutions by computer simulation remains a challenging prospect. System sizes and time scales of processes accessible by MD methods are limited by the current computational power available. Many advances in MD algorithms,[41−43] sampling techniques,[44,45] and computer hardware[46] are driven by the need to study larger systems over longer time scales. By intelligently combining these techniques to accelerate their simulations, researchers can increase their capability by orders of magnitude and do science that was not previously possible.

One approach to extending the size and time scales accessible in MD simulations is coarse graining (CG), which sacrifices the atomic resolution present in all-atom (AA) force fields in exchange for greater computational efficiency. In contrast to AA models, CG models represent molecules as being composed of fictional *beads*, each representing more than one atom. Several CG force fields have been introduced in recent years, which differ

Received: July 27, 2011
Published: October 28, 2011

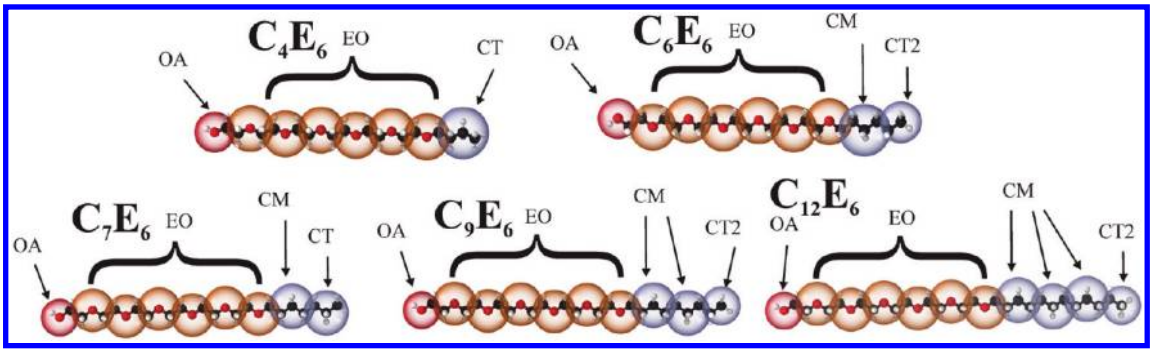

Figure 1. Illustrated representation of the SDK CG model, with CG beads overlaid on the underlying atomistic structure of a series of PEG surfactants considered in this work. Bead types are defined for terminal alcohols (OA), ethoxylate units (EO), nonterminal propyl groups (CM), terminal propyl groups (CT), and terminal ethyl groups (CT2).

in the degree of coarse graining (the number of atoms per bead) and the procedure by which they are parametrized.[1,47,48]

In this work, we will study nonionic surfactant self-assembly with the CG force field of Shinoda, DeVane, and Klein (SDK).[1] This model has been shown to predict the self-assembly of micellar, lamellar, and hexagonal phases of nonionic polyethylene glycol (PEG) surfactant solutions in good agreement with experimental phase diagrams, despite the fact that no phase information was included in the parametrization.[35] The SDK approach to CG parametrization has been applied to many self-assembling systems including ionic surfactants (sulfates, sulfonates)[33] and zwitterionic lipids.[36]

While coarse-grained models offer researchers one means of accelerating the discovery process, further acceleration is possible through the use of advanced computer hardware, such as graphical processing units (GPUs). GPUs are high-performance computer processors designed to accelerate graphical applications (e.g., computer games). In recent years, many scientists have begun to take advantage of the similarity between computer games and scientific simulation—specifically that the bottleneck of both is floating point math—using GPUs to perform scientific simulations.[49] In addition to their strong floating point performance, GPUs are appealing to scientists because of their relatively low cost, with current state-of-the-art models available for ~500 USD. Many researchers in computational chemistry are developing software that uses this advanced computer hardware,[2,50−73] including the implementation of coarse-grained molecular modeling targeted at protein−protein interactions.[74] With two large-scale supercomputers based on GPU technology now available through the NSF Teragrid program[75,76] and three large scale GPU-based machines listed among the four fastest supercomputers in the world,[77] it seems that GPU technology has grown from a promising new development into one of the pillars of high-performance computing.

One rapidly maturing implementation of GPU-based molecular dynamics is HOOMD-Blue.[50] Unlike many existing CPU-based codes that were modified to take advantage of GPU technology, HOOMD-Blue was written from the ground up to take advantage of the advanced features of NVidia GPUs, and it has been shown to provide performance comparable to that of a cluster of tens of CPU cores for medium-sized MD systems (tens to hundreds of thousands of particles).

In this paper, we present an efficient approach to studying self-assembly in micellar solutions using HOOMD-Blue in conjunction with the SDK CG MD force field. In section 2 of this paper, we describe the CG force field employed in this work and our implementation of it into HOOMD-Blue. In section 3, we present data benchmark the performance of HOOMD-Blue in this context, report thermodynamic and structural properties calculated for a series of PEG surfactants, and analyze the convergence and accuracy of these results. In section 4, we draw conclusions.

2. METHODOLOGY

2.1. CG Potential for Aqueous PEG Surfactant Solutions. Before discussing the details of the SDK model, the principles by which it was parametrized are presented. This model was developed to reproduce the thermodynamic and structural properties of complex soft materials.[1] Whenever possible, it has been parametrized to reproduce the experimentally determined thermodynamic properties of bulk materials (e.g., liquid water, hydrocarbons, ethers) and the interfaces between such materials. For example, the SDK model of liquid water was parametrized to faithfully represent the density and surface tension of liquid water under ambient conditions.[78] In addition to experimental data, structural information from AA simulations was also used as target data in the parametrization approach. Note that the SDK model was not parametrized with any knowledge of micellar PEG surfactant systems themselves; thus, all of the results reported in this work are predictions of the model.

The goal of the CG approach is to accurately describe materials without the need to treat the atoms of the system individually, as would be done in traditional AA simulations. As such, the materials are partitioned into CG beads, each of which represent, on average, three heavy atoms and associated hydrogens.[1,35] The PEG surfactants studied here, which contain 49−81 atoms per monomer, are represented by flexible chains whose length vary from 7 to 11 CG beads (see Figure 1). Water normally accounts for the largest consumption of computational time in molecular simulations of aqueous systems; as such, its coarse graining is essential if a large savings of computer time is to be achieved. A previous study has determined that the properties of liquid water listed above can be accurately reproduced with three water molecules combined into a single CG bead.[78]

The SDK potentials employed in this work to study the self-assembly of PEG surfactants involve three energy terms: angles, bonds, and nonbonding Lennard-Jones terms with nonstandard exponents.

Table 1. Simulated Systems

system	concentration (mM)	No. of surfactants	No. of water beads	No. of replicas	total sim. time (μs)
C_4E_6	129	700	96000	20	39.0
	247	1400	96000	4	3.4
	342	2000	96000	4	3.4
	440	2000	72000	4	4.4
	616	2000	48000	20	60.2
	771	2000	36000	4	7.3
	950	2000	24000	4	7.3
C_6E_4	129	700	96000	20	70.9
C_6E_6	128	700	96000	20	68.0
C_6E_8	127	700	96000	20	69.8
C_7E_6	128	700	96000	20	76.4
	65.5	350	96000	4	13.6
	30.3	160	96000	4	12.9
	15.3	80	96000	4	13.3
	7.7	40	96000	4	12.9
	3.8	20	96000	4	13.6
C_9E_6	127	700	96000	20	85.8
$C_{12}E_6$	126	700	96000	20	31.6
Total				200	593.8

The form of the nonbonded Lennard-Jones potentials will be collectively referred to as $U_{LJ}^{CG}(r)$:

$$U_{LJ}^{CG}(r) = \begin{cases} \frac{27}{4}\varepsilon\left[\left(\frac{\sigma}{r}\right)^9 - \left(\frac{\sigma}{r}\right)^6\right] & \text{for } U_{LJ}^{9-6} \\ \frac{3\sqrt{3}}{2}\varepsilon\left[\left(\frac{\sigma}{r}\right)^{12} - \left(\frac{\sigma}{r}\right)^4\right] & \text{for } U_{LJ}^{12-4} \end{cases} \quad (1)$$

where r is the distance between a pair of beads, the minimum of the energy is given by ε, and σ is the distance where $U_{LJ}^{CG}(r) = 0$. Terms of the form U_{LJ}^{12-4} are used for all interactions involving water beads, while terms of the form U_{LJ}^{9-6} are used for interactions of all other pairs.[1]

The total angle potential can be written as

$$U_{ang}^{CG}(\theta_{ijk}, r_{ik}) = U_{ang}(\theta_{ijk}) + U_{soft}(r_{ik}; r_c) \quad (2)$$

where i, j, and k index beads such that i and k are both bonded to j, and r_{ik} is the distance between the pair of particles i and k. U_{ang} is a standard harmonic angle potential, given by

$$U_{ang}(\theta_{ijk}) = \frac{K_{ang}}{2}(\theta_{ijk} - \theta_0)^2 \quad (3)$$

where θ_{ijk} is the angle between the ji and jk vectors, K_{ang} is the angular force constant, and θ_0 is the angle of minimum energy. An additional repulsive potential between particles i and k, $U_{soft}(r)$ is given by

$$U_{soft}(r; r_c) = \begin{cases} U_{LJ}^{CG}(r) - U_{LJ}^{CG}(r_c) & \text{for } r \le r_c \\ 0 & \text{otherwise} \end{cases} \quad (4)$$

where r_c is a cutoff defined by the Lennard-Jones parameters of beads i and k:

$$r_c = \begin{cases} \sigma\left(\frac{3}{2}\right)^{1/3} & \text{for } U_{LJ}^{9-6} \\ \sigma 3^{1/8} & \text{for } U_{LJ}^{12-4} \end{cases} \quad (5)$$

The use of this additional repulsive potential allows for a softer harmonic term while still maintaining a valid representation of excluded volume interactions between atoms i and k.

A simple harmonic bonding potential represents bonds between CG beads:

$$U_{bond}(r_{ij}) = \frac{K_{bond}}{2}(r_{ij} - r_0)^2 \quad (6)$$

where r_{ij} is the distance between beads i and j, r_0 is the minimum energy distance, and K_{bond} is the force constant. All simulation parameters used in this study can be found in the Supporting Information. Note that, because of the fact that harmonic potentials are implemented differently in HOOMD than in many other codes, the expressions for harmonic bond and angle potentials reported here differ from those reported previously[1] by a factor of 1/2. The reported parameters reflect this difference.

2.2. Potential Implementation. In order to run GPU-accelerated MD with the SDK potential, we chose to implement the energy terms associated with this force field into HOOMD-Blue,[2] which is a fast and easy-to-use implementation of MD designed to run on a single GPU. All potentials used in this study have been incorporated into the main HOOMD-Blue distributions, which are available for free download.[79]

Harmonic bonding potentials were implemented in the original HOOMD-Blue distribution; therefore, we needed only to implement the CG angles and nonstandard Lennard-Jones potentials (U_{LJ}^{9-6},U_{LJ}^{12-4}) from the SDK model.[1,35] The GPU implementation for the CG force field potential is straightforward and follows the general framework for the short-ranged nonbonded forces provided in the original paper describing the implementation of HOOMD-Blue (see Algorithm 2 in ref 2). In HOOMD-Blue, a force kernel is launched that is comprised of several threads that run simultaneously. Each thread is associated with an individual particle of the system, for which it accumulates the forces. Positional data for the neighboring atoms is acquired from the fast texture memory of the GPU. In this arrangement, all force terms are calculated multiple times (Newton's third law is not used) to eliminate the need for communication between threads.[2]

2.3. Molecular Dynamics Simulations. To characterize the behavior of nonionic surfactant self-assembly, we have run simulations of aqueous solutions of various PEG surfactants. In total, 200 individual replica simulations were run, the details of which are listed in Table 1. All simulations presented here employed three-dimensional (3D) periodic boundary conditions. They were run in the NPT ensemble with a temperature of 303 K and a pressure of 1 atm, using a Nose-Hoover chain thermostat (τ = 100 ps) and an isotropic Andersen barostat (τ_P = 100 ps). All simulations were carried out using HOOMD-Blue.[2] Most were performed on Longhorn, a cluster of NVidia Quadro FX 5800 GPUs at the Texas Advanced Computing Center (TACC),[75] with the remainder being performed on local resources.

To investigate relationship between micellization behavior and hydrophobic tail length, we choose a series of five PEG surfactants for study: C_4E_6, C_6E_6, C_7E_6, C_9E_6, and $C_{12}E_6$. (Representative configurations are shown in Figure 2; throughout

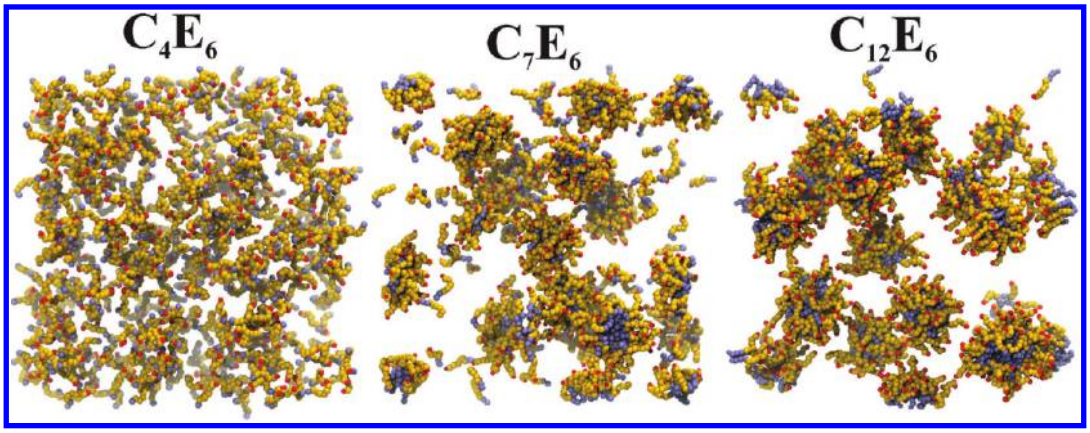

Figure 2. Representative configurations shown for a series of systems differing in hydrocarbon chain length. We illustrate the typical morphology of solutions ranging from nonmicellar (C_4E_6) to strongly micellar ($C_{12}E_6$) PEG surfactants. Water beads have been removed for clarity.

this paper, PEG surfactants will be abbreviated C_xE_y, which x is the length of the hydrophobic tail in carbon atoms and y is the length of the PEG chain in ethoxylate units.) In addition, we considered the dependence of behavior on the surfactant concentration by simulating a series of C_4E_6 and C_7E_6 solutions run at concentrations surrounding the critical micelle concentration (CMC). A study of the dependence of the CMC on the PEG chain length is carried out by considering a series of surfactants of the form C_6E_y. All systems presented here were started from random configurations, with no initial aggregation of the monomers. A time step of 10 fs was used, and trajectory data was saved every 200 ps for subsequent analysis. A total of 20 replicas started from different random initial conditions were run for most systems to improve statistical sampling. In total, this study presents ~0.6 ms of aggregate trajectory data.

2.4. Trajectory Analysis. From the trajectory data, aggregates were identified using a cutoff-cluster method, implemented in similar styles as in previous atomistic[24] and CG studies[35] of surfactant self-assembly. A cutoff of 8.2 Å was chosen for all trajectory data, because it represents the minimum in the radial distribution function of the CG hydrocarbons of micellar PEG from previous simulations using the same model.[35] An analysis of C_7E_6 shows only a subtle dependence of the micelle size distribution on the cutoff over the range between 6 Å and 12 Å (see the Supporting Information).

Because the simulations reported here begin from random, unaggregated arrangements of surfactants, it is necessary to exclude an initial equilibration period from thermodynamic averages. The length of this period depends on the rate of micelle formation and varies from 0.4 μs to 2 μs for the various systems.

In the course of the analysis presented in this paper, it is necessary to define *free monomers*. For the purposes of this paper, "free monomers" are defined to be any monomers that compose aggregates that are smaller than the first minimum in the micelle aggregation number distribution ($N_{agg,min}$; Table 2) for each specific surfactant. To illustrate, monomers composing aggregates smaller than N_{agg} = 15 are considered free monomers for C_6E_6. This definition of "free monomer" includes both true free monomers (those that are completely solvated by water) and small premicellar aggregates, which are believed to exist in micellar solutions at concentrations near the CMC.[80,81]

3. RESULTS AND DISCUSSION

3.1. GPU-Accelerated MD Performance. Before discussing the data collected using our GPU-accelerated MD approach, we report the performance of our implementation. For benchmarking purposes, a system representing a PEG surfactant solution one-quarter the size of our production simulations was chosen: 175 C_9E_6 molecules solvated in 24 000 CG water beads. The performance of HOOMD-Blue running on two different NVidia GPUs—a Quadro FX 5800, as is available on the TACC Longhorn cluster, and a GTX 480, which is a consumer graphics card based on the new Fermi GPU processor—is reported in Figure 3. For comparison, performance is also reported for the widely used and highly optimized CPU-based MD code LAMMPS[82,83] running on the Cray XT5 supercomputer at the National Institute for Computational Science (Kraken). The performance on a single Quadro FX 5800 outperforms 64 processor cores of the XT5 running in parallel, while the newer GTX 480 hardware outperforms all configurations of CPUs tested.

These tests indicate the value of the GPU-acceleration strategy employed by HOOMD-Blue. HOOMD-Blue was designed from the ground up to run on a single GPU, thus eliminating the need for a significant amount of communication between the GPU and the main memory or CPU. While it it is certainly true that massively parallel implementations of MD such as that in LAMMPS are ideal when simulating extremely large systems, for medium-sized systems, such as those simulated in this work (10 000−100 000 particles), a single GPU processor can give performance competitive with a much more expensive CPU cluster. If scientists proceed as if each GPU is its own small CPU

Table 2. Properties of the Micelles Observed in Coarse-Grained (CG) Molecular Dynamics (MD) Simulations[a]

system	conc (mM)	$N_{agg,min}$	$N_{agg,max}$	CMC (mole fract)	$R_{g,max}$ (Å)
C_6E_4	129	15	41	0.99×10^{-3}	15.75
C_6E_6	128	15	24	1.51×10^{-3}	15.75
C_7E_6	128	11	41	3.39×10^{-4}	17.75
C_9E_6	127	4	41	1.19×10^{-5}	18.25
$C_{12}E_6$	126	2	45	1.41×10^{-7}	18.25

[a] The aggregation number at the first minimum of the micelle aggregation number distribution is labeled $N_{agg,min}$; $N_{agg,max}$ is the aggregation number at the maximum; and $R_{g,max}$ is the most probable value of the radius of gyration (R_g). Data for C_4E_6 and C_6E_8 is not included, because there is no clear division between micelles and smaller aggregates for these more-hydrophilic surfactants.

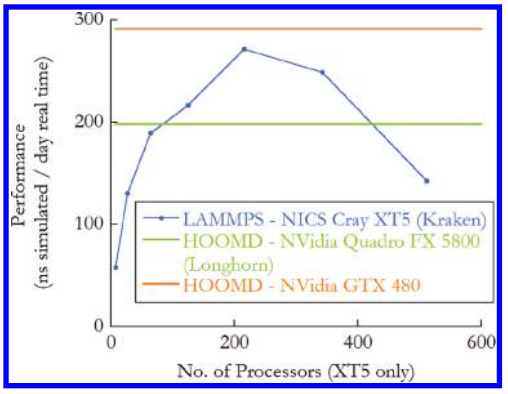

Figure 3. Performance of molecular dynamics (MD) simulations of a CG surfactant systems comprising 175 C_9E_6 molecules solvated in 24 000 CG water beads run using HOOMD-Blue on a single GPU is reported. Results are presented for two different NVidia GPUs: the Quadro FX 5800 (green) and GTX 480 (orange). The performance of LAMMPS, the highly optimized CPU-based MD code,[82,83] running on the NICS Cray XT5 (Kraken) computer cluster is reported as a function of the number of processor cores employed for comparison (blue). The GPU implementation of the SDK model in HOOMD-Blue run on a single NVidia Quadro FX 5800 GPU outperforms LAMMPS running on 64 CPU cores. The same implementation running on a single Fermi-based NVidia GTX 480 card outperforms all configurations of CPUs tested.

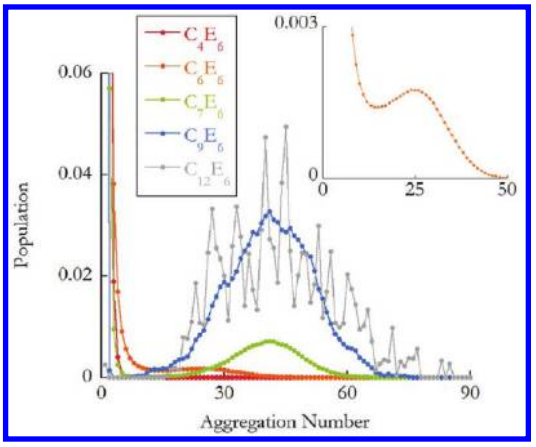

Figure 4. Distributions of micelle aggregation numbers (N_{agg}) of five different surfactant systems at the same concentration. Data are obtained from MD trajectories after a significant equilibration period (0.4−2 μs, depending on the rate of micelle formation). For clarity, the inset shows the C_6E_6 distribution over a narrower range of aggregation number and population. No maximum in the distribution corresponding to stable micelles occurs for C_4E_6, but more micelles form with increasing hydrophobic chain length. The aggregation number at which the distribution is at a maximum increases from 24 for C_6E_6 to 41 for C_7E_6, but then stays relatively constant as the hydrophobic chain length increases to 9 and 12. As can be seen in Figure 5, this is likely due to the fact that these more hydrophobic surfactants would require a longer time to reach equilibrium. The probability of micelles composed of more than 60 monomers rises as the chain length increases from 7 to 12, despite the fact that the maximum of the distribution remains stationary.

cluster, it allows them to dramatically improve their sampling by running multiple replicas in parallel, and this is the strategy that we have employed in this work. Very intriguing, though, is the combination of LAMMPS' massively parallel computation strategy and GPU acceleration, which has shown great promise for extending the capabilities of computers to address questions regarding large-scale molecular systems.[54]

3.2. Size and Structure of Micelles as a Function of Tail Length. From the 0.6 ms of trajectory data collected in this study, we have calculated a variety of thermodynamic properties of nonionic surfactant solutions as a function of the hydrophobic tail length, PEG chain length, and total concentration. A summary of the properties of many of the final micellar solutions can be found in Table 2.

First we investigate the dependence of the structural properties of micelles on the hydrophobic tail length by considering a series of surfactants of the form C_xE_6. All systems were simulated with a mole fraction of monomer of 2.38×10^{-3} (700 surfactant molecules solvated in 96 000 CG water beads). The micelle aggregation number (N_{agg}) distributions of this series are shown in Figure 4. For C_4E_6, the most hydrophilic surfactant considered, the probability of an aggregate decreases monotonically with its N_{agg}, and no aggregates of >12 monomers are observed, indicating that either the concentrations of our simulations is below the CMC or that C_4E_6 does not form micelles. The properties of C_4E_6 will be examined in more detail below.

More hydrophobic surfactants, starting with C_6E_6, exhibit a peak in the distribution corresponding to stable micelles. As has been observed in experiments,[4,84] the peak of the micelle size distribution occurs at larger N_{agg} as the hydrophobic tail length increases from 6 to 7. Surprisingly, however, the maximum of the distribution does not shift to significantly larger N_{agg} as the hydrophobic tail length increases from 7 to 12, despite the fact that experiments[4,84] demonstrate that it does. This discrepancy stems from the fact that the dynamics of micelle growth in these systems are very slow, compared to the time scales accessed by the present simulations. The convergence of the micelle size distributions will be investigated in more detail in the next subsection. The noise observed in the $C_{12}E_6$ is the result of the shorter sampling time and slower evolution of these simulations, compared with the more hydrophilic systems.

Though quantitative information about the micelle size distributions cannot be extracted from our MD data for these more hydrophobic surfactants, one can confirm that the proper qualitative trend—the average micelle aggregation number increases with increasing hydrophobic tail length—is reproduced by considering the time dependence of the average micelle number (Figure 5). Although the micelles observed for surfactants with a hydrophobic tail longer than six carbons continue to grow for the duration of the simulations, the more hydrophilic systems are converging toward lower values of N_{agg}, compared to those that are more hydrophobic.

The shape of the simulated micelles is described in Figure 6, which shows histograms of micelle population as a function of N_{agg} and the eccentricity (deviation from spherical shape). The eccentricity (e) is calculated from the principle moments of inertia, according to the following expression:[29]

$$e = 1 - \frac{I_{min}}{\langle I \rangle} \tag{7}$$

Here, I_{min} represents the principal moment of inertia with the smallest magnitude and $\langle I \rangle$ is the average of all three principal moments. Both the corona and core of the micelles are considered in the moment-of-inertia calculations. The eccentricity of a perfectly spherical object is zero, while infinitesimally thin oblate or prolate objects would have eccentricities approaching one.

The micelles observed in the present simulations generally have eccentricities that deviate from zero, which indicates that

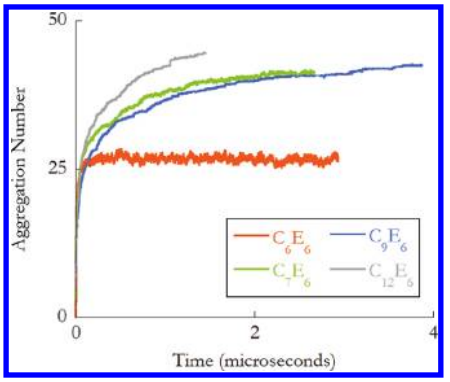

Figure 5. Average micelle aggregation number as a function of time for four surfactant systems, averaged over all replicas. The degree of convergence decreases with increasing hydrophobic tail length, and it appears that more hydrophobic surfactants are approaching larger average aggregation numbers. This qualitative trend is in agreement with the experiment.[4,84]

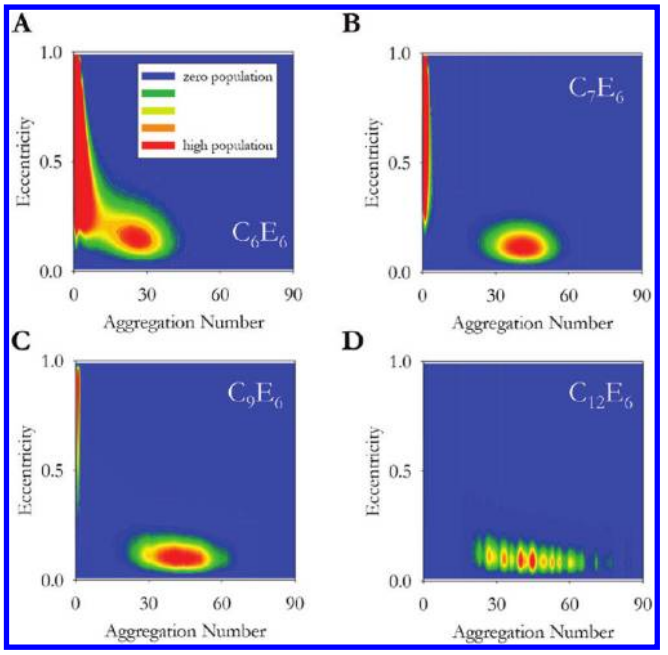

Figure 6. Two-dimensional histograms of micelles as a function of aggregation number and eccentricity (deviation from spherical shape) for four different surfactant systems. In general, aggregates composed of more than 10 monomers are slightly aspherical (eccentricity greater than zero). Trends toward lower eccentricity are observed with increasing hydrocarbon chain length and aggregation number.

they are somewhat aspherical. The larger micelles observed are more spherical, on average, than smaller ones. One would expect this trend to reverse as the micelles transition from spherical to rodlike, but rodlike micelles are not observed in the present simulations.

This trend is also visible in Figure 7, in which one-dimensional slices of the distributions in Figure 6 are shown for clarity. Note that the eccentricity distributions are more sharply peaked near zero for micelles with N_{agg} = 55, compared to those with N_{agg} = 30. In addition, surfactants with longer hydrophobic tails yield more spherical micelles, as can be seen by comparing the one-dimensional eccentricity distributions of C_7E_6 and C_9E_6 at

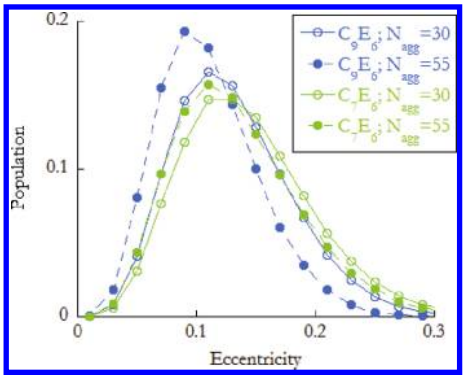

Figure 7. Distribution of eccentricities of micelles differing in aggregation number and the hydrophobic tail length of the component surfactant. As can also be seen in Figure 6, micelles tend to be more spherical (less eccentric) as the length of the hydrophobic chain increases and as the micelles grow larger.

equivalent values of N_{agg}. This trend is in good agreement with the prediction that the radius of a spherical micelle core cannot exceed the length of the hydrocarbon carbon chain.[4]

3.3. Convergence of the Micelle Size Distribution. As noted previously, the peak of the micelle size distribution predicted by our simulations does not change significantly as the hydrophobic tail length increases from 7 to 12, contrary to experimental evidence.[4,84] The source of this discrepancy can be seen in the time evolution of the mean micelle aggregation number of this series of surfactants, presented in Figure 5. Free monomers are excluded when calculating the mean micelle aggregation number. The more-hydrophilic surfactant shown, C_6E_6, reaches an average value of 26 in ~0.5 μs, and subsequently oscillates around this equilibrium size, indicating that this system has likely reached its equilibrium micelle aggregation number distribution. This kinetic equilibrium is supported by the observation of hundreds of micelle fission and fusion processes in these simulations, the kinetics of which will be the subject of a future study. In contrast, after the rapid growth of an initial set of micelles, the average N_{agg} values for the more-hydrophobic systems (C_7E_6 and longer) continue to rise slowly for the duration of the simulations. This indicates that these systems have not reached their equilibrium micelle number distributions, despite the fact that all of the replicas involved in these calculations have a duration of >1 μs, and in the C_7E_6 and C_9E_6 simulations, the replica trajectories average 4 μs each. It appears that, after their initial formation, micelles grow by slow processes (e.g., micelle fusion), which are not accessible, even by the very efficient GPU-accelerated, CG approach employed in this work. However, note that it is only because of the extreme sampling achieved in this study that we are able to see that the average micelles observed in our simulations of C_7E_6 and C_9E_6 continue to grow for the 4-μs duration of our simulations.

In an effort to assess the degree to which these systems remain out of equilibrium, a system composed of four micelles of 175 C_9E_6 molecules solvated in 96 000 water beads was prepared using the Packmol software package.[85] This results in the same concentration (127 mM) as the simulations of C_9E_6 discussed in previous sections. Within the first 2 ns of the simulation, each of these large micelles splits into two smaller ones (see Figure 8A). These eight micelles, with an average micelle number of 86.8, remain stable for 2.0 μs of MD simulation, despite the fact that no aggregates this large are observed in the original simulations (see

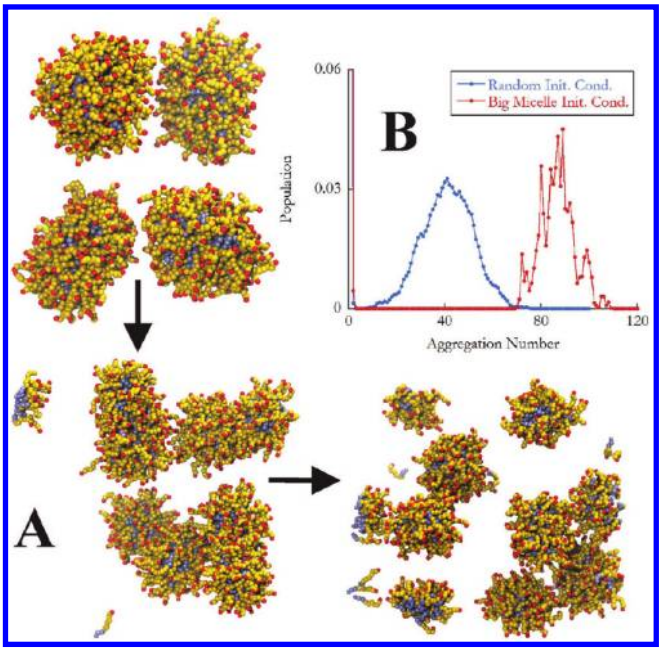

Figure 8. (A) Micelle fission is observed in a simulation that was started from a configuration with four large micelles (175 monomers each) of C_9E_6 (top-left). After these initial fission events (bottom-left), which occurs after only 2 ns of simulations, the resulting micelles remained stable for 2.0 μs (bottom-right). (B) Aggregation number distribution as determined in simulations started from these "big micelle" initial conditions (red), compared with the distribution determined from random, unaggregated initial conditions (blue) at the same total concentration of monomer.

Figure 8B). The discrepancy between the size of stable micelles observed in simulations starting from different initial conditions indicates that advanced sampling techniques, such as replica exchange, are necessary to overcome the large barriers associated with micelle fission and fusion. Such an approach has previously been used in conjunction with GPU-accelerated coarse grained MD in a study of protein−protein interactions.[74] In future work, we will incorporate advanced sampling techniques into our GPU-accelerated coarse-grained MD scheme to more fully sample the equilibrium distribution of micellar solutions.

3.4. Determination of Critical Micelle Concentration. Critical micelle concentrations (CMCs), which are the concentrations above which particular surfactants will form micelles, were predicted from our simulations of micellar solutions at ~128 mM. This is done by measuring the free monomer concentration in these micellar solutions, which analytic theory predicts to be equal to the CMC.[3] The theoretically predicted CMCs of the series of C_xE_6 surfactants are given in Figure 9, along with experimentally determined CMCs for comparison.[84,86,87] As is known, there is tremendous variability in experimental measurements of the CMC, and the experimental measurements of the CMC reported here vary by a factor of 2 in some cases. The strong decrease in the CMC with increasing hydrophobic tail length predicted by the simulations is in good qualitative agreement with experimental results, and the values of the CMC predicted for the more-hydrophilic surfactant systems (C_6E_6 and C_7E_6) are in good quantitative agreement with the experiment. However, for longer hydrophobic tails, the CMC predicted by MD simulation is systematically too small. The simulated CMC deviates from the experimental CMC by a factor of 10 in the worst case ($C_{12}E_6$). It is possible that more-accurate

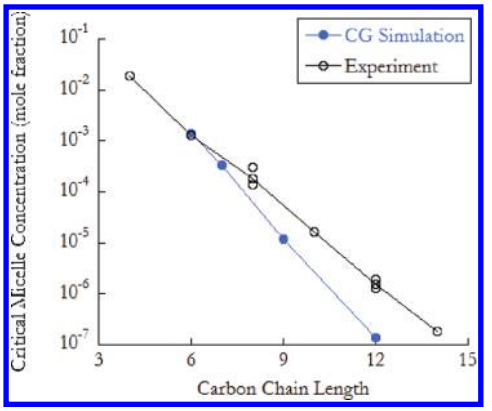

Figure 9. Calculated critical micelle concentrations (CMC) as a function of hydrocarbon chain length are shown in blue, with experimental data[84,86,87] shown in black for comparison. Simulated CMCs are determined from the free monomer concentration of micellar solutions, as described in the text. Agreement with experiment is excellent for short hydrocarbon chains (C_6E_6 and C_7E_6), and the qualitative trend of decreasing CMC with increasing hydrophobicity is reproduced.

results would be obtained in these cases if the simulations were conducted at concentrations closer to the CMC; however, unfortunately, such simulations are not feasible, because of the sheer volume of solvent that would be required to simulate even a single micelle at such low monomer concentration.

Unlike the micelle size distributions previously discussed, the free monomer concentrations used to predict the CMCs appear to have reached converged values relatively early in the simulations. As can be seen in Figure 10, the average number of free monomers observed in each frame of MD trajectory data converges within the first several hundred nanoseconds of simulation. Indeed, the free monomer concentrations reported here appear to be converged.

The dependence of the CMC on the PEG chain length was also calculated. The aggregation number distributions for a series of three surfactant systems of the form C_6E_y are shown in Figure 11. For $y = 8$, only relatively small aggregates are observed, and no minimum is observed in the micelle size distribution, so it is difficult to discriminate between micelles and free monomers. However, there is a strong dependence of the average size of micelles on the PEG chain length, so it is easy to discriminate between micelles and free monomers for C_6E_6 and C_6E_4. In comparison to the length of the hydrophobic tail, which has a very strong effect on the CMC, the length of the hydrophilic PEG chain correlates relatively weakly with the CMC. This trend can be seen in the inset of Figure 11 and is in good agreement with experimental studies of similar PEG surfactant systems, which show a slight increase in the CMC with increasing PEG chain length in surfactants of the forms C_8E_y and $C_{10}E_y$,[87] as well as other simulations.[21]

3.5. Behavior Near the Critical Micelle Concentration. Analytic theory[3] and phenomenological models[4] predict the behavior of surfactant solutions at concentrations surrounding the CMC. At concentrations above the CMC, the concentration of free monomers is expected to be approximately the CMC and remain constant with increasing total concentration. For lower concentration solutions, it is predicted that all monomers will exist as free monomers. However, Vold has suggested that it is more correct to think of the surfactants in solutions approaching the CMC not as free monomers, but as small premicellar aggregates.[80] Many experiments support this suggestion,[88−94]

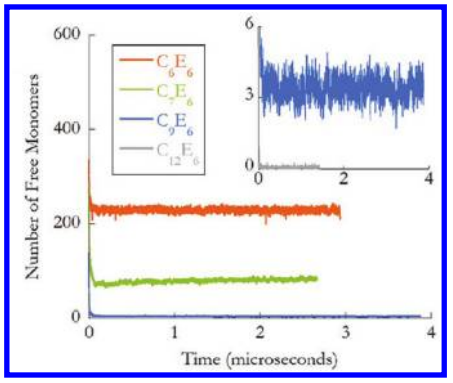

Figure 10. Average number of instantaneous free monomers from simulations of five surfactant systems at the same concentration as a function of time. Values are averaged over all replicas. The inset shows two surfactant systems with a smaller range of numbers of free monomers for clarity. The number of free monomers converges to an average value within <0.2 μs in all cases.

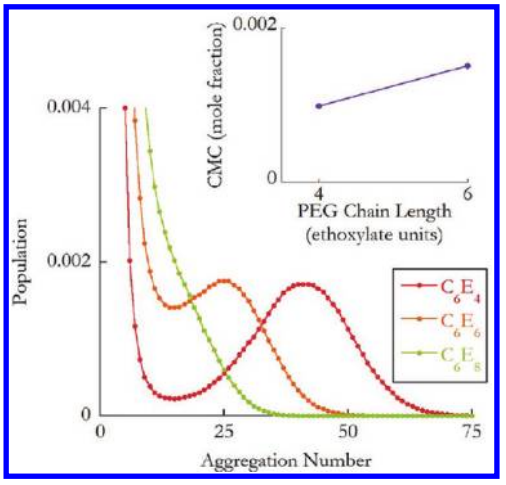

Figure 11. Aggregation number distribution for a series of surfactants differing in the length of the hydrophilic PEG chain, but with constant hydrophobic tail length and concentration. While the PEG chain length has a significant effect on the peak aggregation number, the fraction of monomers forming micelles is relatively constant, indicating that the CMC is relatively insensitive to PEG chain length. No CMC can be determined for C_6E_8, because no peak is observed in the aggregation number (though a shoulder is observed for N_{agg} in the range of 15−25, which corresponds to small, micelle-like aggregates). The CMCs determined for the other two surfactant systems are plotted in the inset. The CMC increases slightly with increasing PEG chain length. This qualitative trend is in good agreement with experimental data.[87]

including a recent dynamic light scattering experiment, demonstrating the existence of such aggregates in PEG surfactant solutions.[81] In a previous publication,[95] the behavior of surfactant solutions at concentrations surrounding the CMC and the prevalence of premicellar aggregates was investigated by conducting sets of simulations spanning a range of concentrations surrounding the CMC for two different PEG surfactants, C_7E_6 and C_4E_6. It was reported that, in C_7E_6 solutions above the CMC, the free monomer concentration (which, in our analysis, is assumed to be a reasonable predictor of the CMC) does not remain constant as the total concentration increases. In fact, it decreases with total concentration, as can be seen in Figure 12. This slow decrease in the free monomer concentration

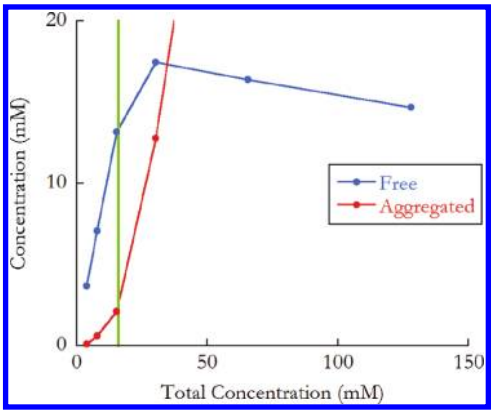

Figure 12. Concentration of unaggregated monomers (those which compose aggregates with N_{agg} = 1; blue) and aggregated monomers (those which compose aggregates with N_{agg} > 1; red) as a function of total C_7E_6 concentration in the neighborhood of the CMC. The CMC, as determined for this model—16.1 mM—is marked by a vertical green line. Two notable deviations from ideal behavior are observed.[95] Above the CMC, the free monomer concentration plateaus, as predicted by analytic theory.[4] However, there is a slight, but unexpected decrease as the total concentration increases, which suggests that a more-accurate CMC can be predicted by calculating the free monomer concentration at a concentration as near to the CMC as possible. In addition, aggregates are observed at a concentration below the CMC, with 8% of monomers aggregated at a concentration of approximately half the CMC.

with increasing total concentration supports the suggestion that a more-accurate CMC can be predicted by simulating at a concentration nearer to the CMC than is feasible for the more-hydrophobic C_9E_6 and $C_{12}E_6$ systems, where the largest deviations of our calculated CMCs from experimental results were observed.

Another noteworthy deviation from ideal behavior, the existence of premicelles, was observed in C_7E_6 solutions below the CMC.[95] In simulations at a concentration less than half of the CMC, 8% of surfactant molecules aggregated, as can be seen in Figure 12. Dimeric structures were observed to be similarly stable to micelles, and significant populations of premicelles composed of between three and nine monomers also were observed.

In Figure 13, we illustrate typical morphologies of C_7E_6 premicelles from a 128 mM solution, with variations in both aggregation number and spherical eccentricity. Along the columns are representative depictions of premicelles ranging in shape from less eccentric (e = 0.125) to highly eccentric (e = 0.65), and along the rows, we show premicelles with aggregation numbers ranging trimers, to pentamers and nonamers, at a constant eccentricity. The diagonal extending from $\{e = 0.65, N_{agg} = 3\}$ to $\{e = 0.125, N_{agg} = 9\}$ roughly corresponds to the most probable eccentricity at a given aggregate size. For all equivalently sized systems, increasing the eccentricity generally results in elongation of the premicelle along its major principal axis, while retaining symmetry along the other two. It is noteworthy that we observed a lack of spherical premicellar structures, as typically used, as a matter of convenience, in the formulation of theoretical models for predicting premicellar thermodynamics.[96]

Deviations from ideal behavior are more severe in aqueous C_4E_6, as can be seen in Figure 14, which presents aggregation number distributions calculated at several concentrations in the vicinity of the experimentally reported CMC, 760 mM.[86] As

the total concentration increases, no peak in the aggregation number distribution develops, despite the fact that aggregates of greater than 100 monomers are observed as the total surfactant concentration approaches 1 M. Similar nonideal behavior is observed if one considers the relationship between the concentrations of smaller aggregates and free monomers and the total surfactant concentration; no sudden leveling of the concentration of free monomers (inset of Figure 14B) or premicellar aggregates (Figure 14B) at a critical concentration is observed. Instead, the concentration of free monomers smoothly transitions from increasing with total surfactant concentration to decreasing at ~500 mM total concentration, in contrast to the sudden change in behavior predicted at the CMC and observed in our simulations of C_7E_6. This indicates that C_4E_6 is not strongly micelle forming and suggests that no CMC can be defined for C_4E_6 in water. Although a CMC for C_4E_6 has previously been inferred from surface tension experiments,[86] no raw data was reported, so it is impossible to assess the degree to which the change in behavior at the reported CMC is sudden. Given the large aggregates observed in our simulations, it would not be surprising if the surface tension of C_4E_6 does not depend strongly on the concentration around the experimentally determined CMC (760 mM), even if no critical behavior is observable. To the authors' knowledge, no other measurement of the CMC of C_4E_6 has been reported in the literature.

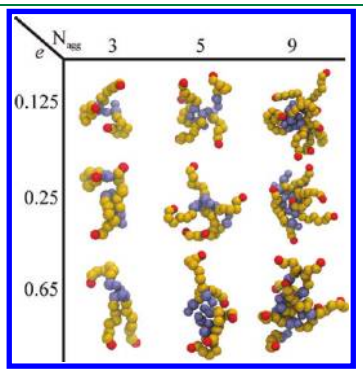

Figure 13. Morphology of premicellar aggregates as a function of aggregation number (N_{agg} = 3, 5, 9) and spherical eccentricity (e = 0.125, 0.25, 0.65; see eq 7). The diagonal extending from the lower left to the top right follows the peak in the respective system's eccentricity distribution. By increasing the eccentricity (columns), premicellar aggregates tend to elongate along a major principal axis for all three system. Note that perfectly spherical premicelles are not observed at any aggregation size.

4. CONCLUSIONS

In this paper, we presented a study using GPU-accelerated coarse-grained (CG) molecular dynamics (MD) simulations to investigate the properties of micellar solutions of nonionic surfactants. In order to carry out this study, a GPU-accelerated implementation of the SDK force field[1] was added to the HOOMD-Blue GPU-accelerated MD software package.[2] The performance of a 25 000 particle MD simulation on a single GPU was comparable to that obtained using the LAMMPS MD software package[82,83] running on an optimally sized computer cluster comprising tens of CPU cores. All code developed and used in this work is available for free download with the current production release of the HOOMD-Blue GPU-accelerated MD software package.[79]

The combined efficiency afforded us by the CG model and GPU hardware allowed us to undertake an unprecedented study of surfactant self-assembly, collecting a total of 0.6 ms of trajectory data in 200 replica simulations. From this data, we calculated and reported many different thermodynamic and structural properties. Converged critical micelle concentrations (CMCs) exhibited the qualitatively correct dependence on the length of the hydrophobic tail and hydrophilic PEG headgroup. Quantitative agreement with experiment was achieved for more-hydrophilic surfactant systems (C_6E_6 and C_7E_6), while the CMCs of more hydrophobic surfactants were underestimated significantly. For C_7E_6, it has been previously reported that the free monomer concentration decreases as the total monomer concentration increases beyond the CMC,[95] in contrast to widely used models that predict it to remain relatively constant. This trend suggests that errors in the CMCs of the more hydrophobic

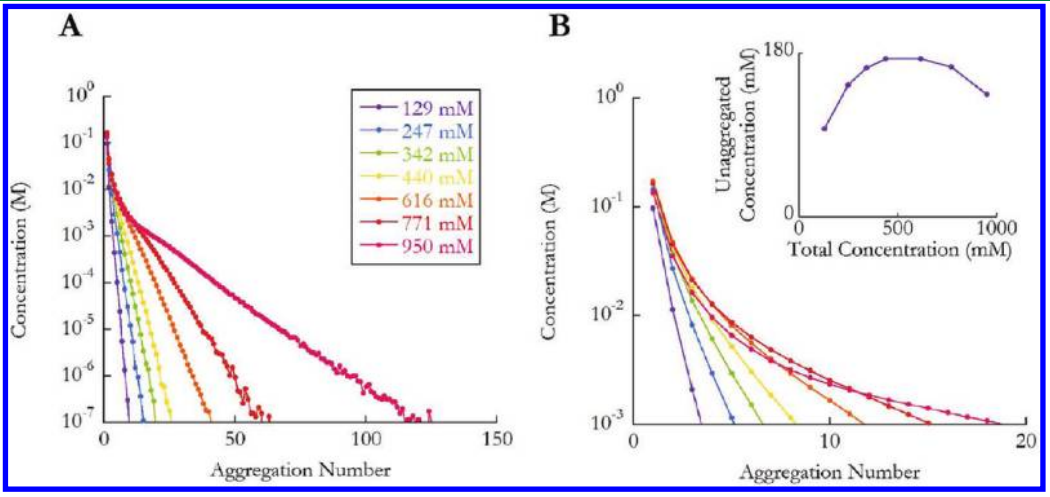

Figure 14. (A) Distribution of micelle aggregation numbers for aqueous C_4E_6 surfactant systems at various total surfactant concentrations. (B) Enlarged view showing the concentration of small premicellar aggregates. The concentration of unaggregated monomers (those which compose aggregates with N_{agg} = 1), as a function of total monomer concentration in the neighborhood of a previously reported CMC (760 mM),[30] is shown in the inset of Panel B. Unlike C_7E_6 (see Figure 12), and despite the fact that large aggregates exist at high concentration, C_4E_6 does not exhibit a sharp change in behavior at a particular concentration (CMC). In addition, it is aggregation number distribution develop a peak at high concentration more similar to the more-hydrophobic surfactants (see Figure 4).

surfactants may result from the fact that the simulations are carried out at concentrations much above the CMC. For the most-hydrophilic surfactant studied, C_4E_6, no sharp change in behavior is seen at any concentration, suggesting that no CMC can be defined for this system.

The average micelle aggregation numbers determined from our simulations increase with hydrophobic chain length, which is in agreement with experimental results. However, even with the extreme sampling achieved in this work, equilibrium micelle size distributions are achieved for only the most-hydrophilic surfactant systems. In fact, it is only because of the large trajectory data set collected that the slow micellar growth that continues for the duration of our simulations can be observed at all. In future work, we will examine the dynamics of this growth and employ advanced sampling techniques in conjunction with our GPU-accelerated CG scheme to attempt to sample true equilibrium distributions for the more challenging hydrophobic surfactant systems.

■ ASSOCIATED CONTENT

Supporting Information. An additional Supporting Information file is available, containing the following: tables of force-field parameters; radius of gyration distributions for various micellar systems; plots showing the sensitivity of the micelle size distribution, with respect to the clustering cutoff; and a sample HOOMD input file for running a PEG surfactant system with the SDK model. This information is available free of charge via the Internet at http://pubs.acs.org.

■ AUTHOR INFORMATION

Corresponding Author

*E-mail: mlklein@temple.edu.

Author Contributions

▽D.N.L. and B.G.L. contributed equally to this work.

■ ACKNOWLEDGMENT

The authors gratefully acknowledge many useful discussions with Arben Jusufi, Joshua Anderson, Alex Travesset, Athanassios Panagiotopoulos, Samantha Sanders, and Steve Barr. We are also extremely grateful to Joshua Anderson and Paul Navratil for technical assistance. This work was supported by the National Science Foundation (under Grant Nos. CHE-09-46358 and CNS-09-58854) and through TeraGrid resources provided by the Texas Advanced Computing Center, National Center for Supercomputer Applications, and National Institute for Computational Science (under Grant Nos. TG-MCA93S020 and TG-ASC090088). R.D. and M.L.K. would also like to thank The Procter & Gamble company for generous support.

■ REFERENCES

(1) Shinoda, W.; DeVane, R.; Klein, M. L. *Mol. Simul.* **2007**, *33*, 27–36.
(2) Anderson, J. A.; Lorenz, C. D.; Travesset, A. *J. Comput. Phys.* **2008**, *227*, 5342–5359.
(3) Israelachvili, J. N. *Intermolecular and Surface Forces*; Harcourt Brace: London, 1992.
(4) Tanford, C. *The Hydrophobic Effect: Formation of Micelles and Biological Membranes*; John Wiley & Sons: New York, 1973.
(5) Xia, Y. N.; Whitesides, G. M. *Annu. Rev. Mater. Sci.* **1998**, *28*, 153–184.
(6) Kato, T.; Mizoshita, N.; Kishimoto, K. *Angew. Chem., Int. Ed.* **2006**, *45*, 38–68.
(7) Klein, M. L.; Shinoda, W. *Science* **2008**, *321*, 798–800.
(8) Marrink, S. J.; de Vries, A. H.; Tieleman, D. P. *Biochim. Biophys. Acta* **2009**, *1788*, 149–168.
(9) Watanabe, K.; Ferrario, M.; Klein, M. L. *J. Phys. Chem.* **1988**, *92*, 819–821.
(10) Watanabe, K.; Klein, M. L. *J. Phys. Chem.* **1989**, *93*, 6897–6901.
(11) Smit, B.; Hilbers, P. A. J.; Esselink, K.; Rupert, L. A. M.; van Os, N. M.; Schlijper, A. G. *Nature* **1990**, *348*, 624–625.
(12) Smit, B.; Hilbers, P. A. J.; Esselink, K.; Rupert, L. A. M.; van Os, N. M.; Schlijper, A. G. *J. Phys. Chem.* **1991**, *95*, 6361–6368.
(13) Karaborni, S.; Esselink, K.; Hilbers, P. A. J.; Smit, B.; Karthauser, J.; van Os, N. M.; Zana, R. *Science* **1994**, *266*, 254–256.
(14) Karaborni, S.; Smit, B. *Curr. Opin. Colloid Interface Sci.* **1996**, *1*, 411–415.
(15) Abel, S.; Dupradeau, F.-Y.; Raman, E. P.; MacKerell, A. D.; Marchi, M. *J. Phys. Chem.* **2011**, *115B*, 487–499.
(16) Amani, A.; York, P.; de Waard, H.; Anwar, J. *Soft Matter* **2011**, *7*, 2900–2908.
(17) Bruce, C. D.; Berkowitz, M. L.; Perera, L.; Forbes, M. D. E. *J. Phys. Chem.* **2002**, *106B*, 3788–3793.
(18) Fujiwara, S.; Itoh, T.; Hashimoto, M.; Horiuchi, R. *J. Chem. Phys.* **2009**, *130*, 144901.
(19) Gao, J.; Ge, W.; Hu, G.; Li, J. *Langmuir* **2005**, *21*, 5223–5229.
(20) Garde, S.; Yang, L.; Dordick, J. S.; Paulaitis, M. E. *Mol. Phys.* **2002**, *100*, 2299–2306.
(21) Jusufi, A.; Sanders, S.; Klein, M. L.; Panagiotopoulos, A. Z. *J. Phys. Chem.* **2011**, *115B*, 990–1001.
(22) Lazaridis, T.; Mallik, B.; Chen, Y. *J. Phys. Chem.* **2005**, *109B*, 15098–15106.
(23) Marrink, S. J.; Tieleman, D. P.; Mark, A. E. *J. Phys. Chem.* **2000**, *104B*, 12165–12173.
(24) Sammalkorpi, M.; Sanders, S.; Panagiotopoulos, A. Z.; Karttunen, M.; Haataja, M. *J. Phys. Chem.* **2011**, *115B*, 1403–1410.
(25) Stephenson, B. C.; Stafford, K. A.; Beers, K. J.; Blankschtein, D. *J. Phys. Chem.* **2008**, *112B*, 1641–1656.
(26) Tieleman, D. P.; van der Spoel, D.; Berendsen, H. J. C. *J. Phys. Chem.* **2000**, *104B*, 6380–6388.
(27) Chowdhary, J.; Ladanyi, B. M. *J. Phys. Chem.* **2009**, *113B*, 15029–15039.
(28) Salaniwal, S.; Cui, S. T.; Cochran, H. D.; Cummings, P. T. *Langmuir* **2001**, *17*, 1773–1783.
(29) Senapati, S.; Keiper, J. S.; DeSimone, J. M.; Wignall, G. D.; Melnichenko, Y. B.; Frielinghaus, H.; Berkowitz, M. L. *Langmuir* **2002**, *18*, 7371–7376.
(30) Denham, N.; Holmes, M. C.; Zvelindovsky, A. V. *J. Phys. Chem.* **2011**, *115B*, 1385–1393.
(31) Drouffe, J. M.; Maggs, A. C.; Leibler, S. *Science* **1991**, *254*, 1352–1356.
(32) Goetz, R.; Lipowsky, R. *J. Chem. Phys.* **1998**, *108*, 7397–7409.
(33) He, X.; Shinoda, W.; DeVane, R.; Anderson, K. L.; Klein, M. L. *Chem. Phys. Lett.* **2010**, *487*, 71–76.
(34) Izvekov, S.; Voth, G. A. *J. Phys. Chem.* **2009**, *113B*, 4443–4455.
(35) Shinoda, W.; DeVane, R.; Klein, M. L. *Soft Matter* **2008**, *4*, 2454–2462.
(36) Shinoda, W.; DeVane, R.; Klein, M. L. *J. Phys. Chem.* **2010**, *20*, 6836–6849.
(37) Baoukina, S.; Monticelli, L.; Risselada, H. J.; Marrink, S. J.; Tieleman, D. P. *Proc. Natl. Acad. Sci. U.S.A.* **2008**, *105*, 10803–10808.
(38) Sammalkorpi, M.; Karttunen, M.; Haataja, M. *J. Am. Chem. Soc.* **2008**, *130*, 17977–17980.
(39) Anderson, J. A.; Travesset, A. *Macromolecules* **2006**, *39*, 5143–5151.
(40) Phillips, C. L.; Iacovella, C. R.; Glotzer, S. C. *Soft Matter* **2010**, *6*, 1693–1703.
(41) Bowers, K. J.; Chow, E.; Xu, H.; Dror, R. O.; Eastwood, M. P.; Gregersen, B. A.; Klepeis, J. L.; Kolossvary, I.; Moraes, M. A.; Sacerdoti,

F. D.; Salmon, J. K.; Shan, Y.; Shaw, D. E. In *Proceedings of the 2006 ACM/IEEE Conference on Supercomputing*; IEEE Press: Piscataway, NJ, 2006; pp 11−17.
(42) Darden, T.; York, D.; Pedersen, L. *J. Chem. Phys.* **1993**, *98*, 10089–10092.
(43) Tuckerman, M.; Berne, B. J.; Martyna, G. J. *J. Chem. Phys.* **2008**, *97*, 1990.
(44) Christen, M.; Van Gunsteren, W. F. *J. Comput. Chem.* **2008**, *29*, 157–166.
(45) Liwo, A.; Czaplewski, C.; Oldziej, S.; Scheraga, H. A. *Curr. Opin. Struct. Biol.* **2008**, *18*, 134–139.
(46) Shaw, D. E. *Commun. ACM* **2008**, *51*, 91–97.
(47) Izvekov, S.; Voth, G. A. *J. Phys. Chem.* **2005**, *109B*, 2469–2473.
(48) Marrink, S. J.; Risselada, H. J.; Yefimov, S.; Tieleman, D. P.; de Vries, A. H. *J. Phys. Chem.* **2007**, *111B*, 7812–7824.
(49) Owens, J. D.; Houston, M.; Luebke, D.; Green, S.; Stone, J. E.; Phillips, J. C. *Proc. IEEE* **2008**, *96*, 879–899.
(50) Anderson, A. G.; Goddard, I., W. A.; Schroder, P. *Comput. Phys. Commun.* **2007**, *177*, 298–306.
(51) Asadchev, A.; Allada, V.; Felder, J.; Bode, B. M.; Gordon, M. S.; Windus, T. L. *J. Chem. Theory Comput.* **2010**, *6*, 696–704.
(52) Bauer, B. A.; Davis, J. E.; Taufer, M.; Patel, S. *J. Comput. Chem.* **2011**, *32*, 375–385.
(53) Brown, P.; Woods, C.; McIntosh-Smith, S.; Manby, F. R. *J. Chem. Theory Comput.* **2008**, *4*, 1620–1626.
(54) Brown, M.; Wang, P.; Plimpton, S. J.; Tharrington, A. N. *Comput. Phys. Commun.* **2011**, *182*, 898–911.
(55) Eastman, P.; Pande, V. S. *J. Chem. Theory Comput.* **2010**, *6*, 434–437.
(56) Elsen, E.; Houston, M.; Vishal, V.; Darve, E.; Hanrahan, P.; Pande, V. In *Proceedings of the 2006 ACM/IEEE Conference on Supercomputing*; IEEE Press: Piscataway, NJ, 2006; p 188.
(57) Friedricks, M. S.; Eastman, P.; Vaidyanathan, V.; Houston, M.; LeGrand, S.; Beberg, A. L.; Ensign, D. L.; Brums, C. M.; Pande, V. S. *J. Comput. Chem.* **2009**, *30*, 864–872.
(58) Harvey, M. J.; Giupponi, G.; De Fabritiis, G. *J. Chem. Theory Comput,* **2009**, *5*, 1632–1639.
(59) Harvey, M. J.; De Fabritiis, G. *J. Chem. Theory Comput.* **2009**, *5*, 2371–2377.
(60) Jha, P. K.; Sknepnek, R.; Guerrero-Garcia, G. I.; de la Cruz, M. O. *J. Chem. Theory Comput.* **2010**, *6*, 3058–3065.
(61) Narumi, T.; Yasuoka, K.; Taiji, M.; Hoefinger, S. *J. Comput. Chem.* **2009**, *30*, 2351–2357.
(62) Olivares-Amaya, R.; Watson, M. A.; Edgar, R. G.; Vogt, L.; Shao, Y.; Aspuru-Guzik, A. *J. Chem. Theory Comput.* **2010**, *6*, 135–144.
(63) Peng, L.; Nomura, K.; Oyakawa, T.; Kalia, R. K.; Nakano, A.; Vashishta, P. *14th International Euro-Par Conference*; Springer−Verlag: Berlin, Germany, 2008; pp 763−777.
(64) Phillips, J. C.; Stone, J. E.; Schulten, K. In *Proceedings of the 2008 ACM/IEEE Conference on Supercomputing*; IEEE Press: Piscataway, NJ, 2008; p 1−9.
(65) Rodrigues, C. I.; Hardy, D. J.; Stone, J. E.; Schulten, K.; Hwu, W.-M. W. In *Proceedings of the 2008 Conference on Computing Frontiers*; ACM: New York, 2008; pp 273−282.
(66) Stone, J. E.; Saam, J.; Hardy, D. J.; Vandivort, K. L.; Hwu, W.-M. W.; Schulten, K. In *Proceedings of the 2nd Workshop on General Purpose Processing on Graphics Processing Units*; ACM International Conference Proceeding Series; ACM: Washington, DC, 2009; Vol. 383; pp 9−18.
(67) Stone, J. E.; Phillips, J. C.; Freddolino, P. L.; Hardy, D. J.; Trabuco, L. G.; Schulten, K. *J. Comput. Chem.* **2007**, *28*, 2618–2640.
(68) Sukhwani, B.; Herbordt, M. C. *Proceedings of the 2nd Workshop on General Purpose Processing on Graphics Processing Units*; ACM: Washington, DC, 2009; Vol. 383; pp 19−27.
(69) Ufimtsev, I. S.; Martinez, T. J. *Comput. Sci. Eng.* **2008**, *10*, 26–34.
(70) Ufimtsev, I. S.; Martinez, T. J. *J. Chem. Theory Comput.* **2009**, *5*, 1004–1015.
(71) Vogt, L.; Olivares-Amaya, R.; Kermes, S.; Shao, Y.; Amador-Bedolla, C.; Aspuru-Guzik, A. *J. Phys. Chem.* **2008**, *112A*, 2049–2057.
(72) Watson, M. A.; Olivares-Amaya, R.; Edgar, R. G.; Aspuru-Guzik, A. *Comput. Sci. Eng.* **2010**, *12*, 40–51.
(73) Yasuda, K. *J. Chem. Theory Comput.* **2008**, *4*, 1230–1236.
(74) Tunbridge, I.; Best, R. B.; Gain, J.; Kuttel, M. M. *J. Chem. Theory Comput.* **2010**, *6*, 3588–3600.
(75) *Texas Advanced Computing Center: Visualization*, http://www.tacc.utexas.edu/resources/visualization/.07/01/2011.
(76) *Intel 64 T Linux Cluster Lincoln*, http://www.ncsa.illinois.edu/UserInfo/Resources/Hardware/Intel64TeslaCl.
(77) *TOP500 Supercomputing Sites*, http://www.top500.org/lists/2010/11.12/01/2010, accessed November 2010.
(78) He, X.; Shinoda, W.; DeVane, R.; Klein, M. L. *Mol. Phys.* **2010**, *108*, 2007–2020.
(79) *HOOMD-Blue Download*, http://codeblue.umich.edu/hoomd-blue/download.html (accessed July 1, 2011).
(80) Vold, M. *Langmuir* **1992**, *8*, 1082–1085.
(81) Lee, Y.-C.; Liu, H.-S.; Lin, S.-Y.; Huang, H.-F.; Wang, Y.-Y.; Chou, L.-W. *J. Chin. Inst. Chem. Eng.* **2008**, *39*, 75–83.
(82) Plimpton, S. *J. Comput. Phys.* **1995**, *117*, 1–19.
(83) *LAMMPS*, http://lammps.sandia.gov., accessed July 1, 2011.
(84) Balmbra, R. R.; Clunie, J. S.; Corkill, J. M.; Goodman, J. F. *Trans. Faraday Soc.* **1964**, *60*, 979–985.
(85) Martinez, L.; Andrade, R.; Birgin, E. G.; Martínez, J. M. *J. Comput. Chem.* **2009**, *30*, 2157–2164.
(86) Elworthy, P. H.; Florence, A. T. *Kolloid Z. Z. Polym.* **1964**, *195*, 23–27.
(87) Corkill, J. M.; Goodman, J. F.; Harrol, S. P. *Trans. Faraday Soc.* **1964**, *60*, 202–207.
(88) Niu, S.; Gopidas, K. R.; Turro, N. J.; Gabor, G. *Langmuir* **1992**, *8*, 1271–1277.
(89) Menger, F. M.; Littau, C. A. *J. Am. Chem. Soc.* **1993**, *115*, 10083–10090.
(90) Sakai, T.; Kaneko, Y.; Tsujii, K. *Langmuir* **2006**, *22*, 2039–2044.
(91) Cui, X.; Mao, S.; Liu, M.; Yuan, H.; Du, Y. *Langmuir* **2008**, *24*, 10771–10775.
(92) Barnadas-Rodriguez, R.; Estelrich, J. *J. Phys. Chem.* **2009**, *113B*, 1972–1982.
(93) Sowmiya, M.; Tiwari, A. K.; Saha, S. K. *J. Colloid Interface Sci.* **2010**, *344*, 97–104.
(94) Beija, M.; Fedorov, A.; Charreyre, M. T.; Marinho, J. M. G.; Jose, M. G. *J. Phys. Chem.* **2010**, *114B*, 9977–9986.
(95) LeBard, D. N.; Levine, B. G.; DeVane, R.; Shinoda, W.; Klein, M. L. *Chem. Phys. Lett.* **2011**, submitted for publication. (See Supporting Information.)
(96) Hadgiivanova, R.; Diamant, H. *J. Phys. Chem. B* **2007**, *111B*, 8854–8859.